Cell Biol Toxicol (2021) 37:15–34
https://doi.org/10.1007/s10565-020-09520-w

ORIGINAL ARTICLE

Roles of acyl-CoA synthetase long-chain family member 5 and colony stimulating factor 2 in inhibition of palmitic or stearic acids in lung cancer cell proliferation and metabolism

Linlin Zhang · Jiapei Lv · Chengshui Chen · Xiangdong Wang

Received: 27 December 2019 / Accepted: 28 February 2020 / Published online: 28 April 2020

Abstract Lung cancer is a heterogeneous and complex disease with the highest incidence and mortality rate. The present study aims at defining the lung cancer phenome specificity of lipidomic profiles, screening target lipid-dependent transcriptional alternations, identifying target lipid-associated target genes, and exploring molecular mechanisms. Lung cancer-specific and lung cancer subtype-specific target lipids palmitic acid (C16:0) and stearic acid (C18:0) were found as target lipids by integrating clinical phenomics, lipidomics, and transcriptomics and exhibited antiproliferative effects in sensitive cells. The metabolism-associated gene ACSL5 or inflammation-associated gene CCL3 was identified in lung adenocarcinoma or small lung cancer cells, respectively. C16:0 or C18:0 could upregulate ACSL5 or CSF2 expression in a time- and dose-dependent pattern, and the deletion of both genes led to the insensitivity of cells. Target lipids increased the expression of PDK4 gene in different patterns and inhibited cell proliferation through alterations of intracellular energy. Thus, our data provide a new strategy to investigate the trans-points between clinical and phenomics and lipidomics and target lipid-associated molecular mechanisms to benefit from the discovery of new therapies.

Keywords Clinical phenome · Lipidomics · Lung cancer · ACSL5 · CSF2

Abbreviations

eQTL	Expression quantitative trait locus
GEO	Gene Expression Omnibus
LPC	Lysophosphatidylcholine
LPE	Lysophosphatidylethanolamine
PA	Phosphatidic acid
PC	Phosphatidylcholine
PE	Phosphatidylethanolamine
PG	Phosphatidylglycerol
PI	Phosphatidylinositol
PS	Phosphatidylserine

Introduction

Lung cancer is a heterogeneous, complex, multifactorial, and refractory disease with the highest incidence and mortality rate. Major functions of lung cancer cells are maintained by multiple nutrients, e.g., lipids. Lipid metabolic disorders occur in many diseases, although the specificity of disease types, severities, and durations are still unclear

Linlin Zhang and Jiapei Lv contributed equally to this work.

Electronic supplementary material The online version of this article (https://doi.org/10.1007/s10565-020-09520-w) contains supplementary material, which is available to authorized users.

L. Zhang · C. Chen (✉) · X. Wang
Department of Respiratory Medicine, Wenzhou Medical University, Wenzhou, Zhejiang Province, China
e-mail: wzchencs@163.com

J. Lv · X. Wang (✉)
Zhongshan Hospital Institute of Clinical Science, Fudan University Shanghai Medical School, Shanghai, China
e-mail: xdwang@fuccb.com

(Qiao and Wang 2019; Chirshev et al. 2019; Qi et al. 2019). Our previous study demonstrated that circulating lipidomic profiles of patients with lung cancer obviously differed from those of healthy individuals and varied among subtypes of lung cancers (Lv et al. 2018a). Some of the lipid species with lung cancer-specific or subtype-specific characteristics are proposed to be disease biomarkers to monitor the response to therapy, although the exact mechanisms by which selected lipids contribute to cancer cell growth need to be further explored (Lin et al. 2017). With the rapid development of the methodology for lipid measurements, the number of studies on lipidomic profiles of disease samples is increasing and calls for special attention on regulatory mechanisms.

Clinical lipidomics is an extension of lipidomics to integrate lipidomic profiles and networks with clinical phenomes as well as with cell and organ functions (Yan et al. 2018; Lv et al. 2018b). Lin et al. selected target lipids from lipidomic profiles of liver cancer cells and found that palmitic acid (C16:0)-containing glycerophospholipids could downregulate cancer growth and metastasis by regulating cell membrane fluidity and limited glucose metabolism (Lin et al. 2017). The present study aims at further defining the lung cancer phenome specificity of lipidomic profiles, screening target lipid-dependent transcriptional alternations, identifying target lipid-associated target genes, and exploring molecular mechanisms how selected target lipids and genes regulate lung cancer cell biobehaviors. Lipidomic profiles were integrated with clinical phenomes to select two phenome-associated lipid elements through clinical trans-omics strategy (Zhang et al. 2018): palmitic acid (C16:0) and stearic acid (C18:0), respectively. Then, the biological effects of selected target lipid species were evaluated on various lung cancer cells and defined target lipid-sensitive lung cancer cells, lung alveolar adenocarcinoma epithelial cells (ADC) (A549), and small cell lung carcinoma (SCLC) cells (H1668), as shown in Fig. 1. Target lipid-associated genes in lung cancer cells are screened by transcriptional sequencing, from which acyl-CoA synthetase long-chain family member 5 (ACSL5) in ADC cells and colony stimulating factor 2 (CSF2) in SCLC cells are identified, respectively. The roles of target lipid-associated genes are further investigated.

Materials and methods

Materials

Lipid extraction (Bligh and Dyer 1959) solvents used were HPLC grade including chloroform, methanol, hexane and ammonium acetate, and isopropanol (Billerica, MA, USA). Reagents with analytical grade were purchased from Sigma-Aldrich (St. Louis, MO, USA), and stearic acid (C18:0) and palmitic acid (C16:0) were from Sigma-Aldrich. Glass tubes (Kimble, USA) and internal standard cocktails were from Avanti Lipids Polar (Alabaster, AL, USA), including phosphatidylcholine (d7-PC15:0–18:1), phosphatidylethanolamine (d7-PE15:0–18:1), phosphatidylserine (d7-PS15:0–18:1), phosphatidylglycerol (d7-PG15:0–18:1), phosphatidylinositol (d7-PI15:0–18:1), phosphatidic acid (d7-PA15:0–18:1), lysophosphatidylcholine (d7-LPC18:1), lysophosphatidylethanolamine (d7-LPE18:1), cholesteryl ester (d7-Chol Ester18:1), monoglyceride (d7-MG18:1), diacylglycerol (d7-DG15:0–18:1), triglyceride (d7-15:0-TG15:0–18:1), sphingomyelin (d9-SM18:1), and cholesterol (d7). Lipid internal standard was prepared at an amount of 10 μL to each sample.

Patient blood sampling

Blood was harvested from patients with lung squamous cell carcinoma (SCC), lung adenocarcinoma (ADC), or small cell lung cancer (SCLC), as well as from noncancer individuals using EDTA anti-condensation pipe. Lung cancer patients were recruited according to the WHO definition of lung cancer and the histopathological diagnostic criteria and scored for disease staging according to UICC staging. The healthy were over 18 years of age, with normal physical examination and routine laboratory examination and without other lung underlying diseases and risk factors, including smoking, biofuel exposure, or dust or chemical exposure history. Those with hypertension, diabetes, hyperlipidemia, and other cancers were excluded. The study was approved by Zhongshan Hospital Ethics Committee of Fudan University. Blood was taken in the morning after fasting at night from the study patients and healthy individuals who had not used any drugs to avoid the effects of diet and drugs on blood test results. The patients were informed about the objective of the study and provided consent for the analysis of lipid

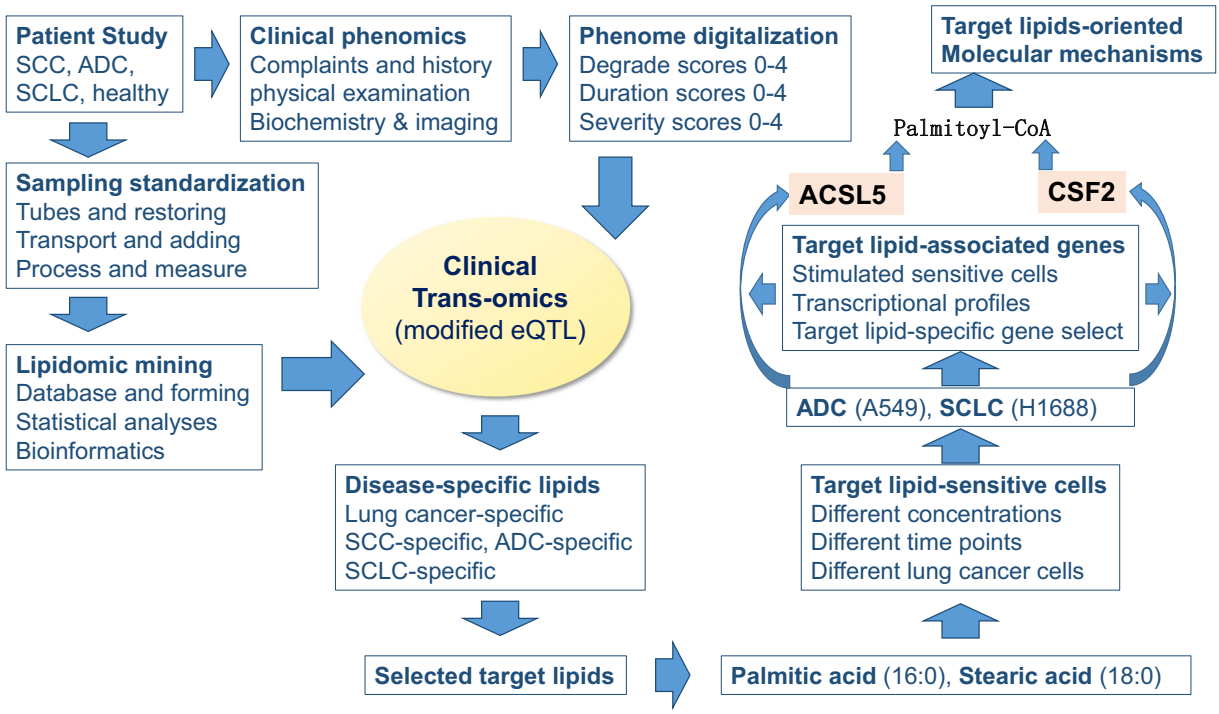

Fig. 1 Clinical trans-omics workflow. After collecting clinical samples from three lung cancer subtypes and healthy people, on the one hand, collecting clinical phenotypic information of patients includes digital scoring of multiple items such as patient complaints, physical examinations, laboratory tests, and cancer grade scores, and scores from 0 to 4 according to the degree of symptoms. On the other hand, clinical samples were detected by mass spectrometry after standardized processing, as well as subsequent data processing and analysis. The clinical digital information and mass spectrometry data were processed by the *eQTL* model, the correlation between the two was analyzed, and targeted lipid molecules were screened out. In this study, we selected palmitic acid and stearic acid for subsequent research and screened their sensitive cells as well as related genes to further explore their molecular mechanisms

data with ethical code B2018-187. Twenty-six patients and 8 healthy people were recruited in the study, among which 9 were SCC, 9 were ADC, and 8 were SCLC. There were 7 men and 2 women in SCC with a mean age of 65.67; in ADC, there are 4 men and 5 women with a mean age of 70.11; and in SCLC, 7 men and 1 woman were enlisted with a mean age of 68.25. After blood sampling, plasma was prepared with centrifugation at 3000 rpm for 10 min at room temperature and then stored at − 80 °C for further measurement.

Lipid extraction

Plasma lipids were extracted, as reported previously (Bligh and Dyer 1959). Briefly, 200 μL plasma was taken into the glass tube, added with 10 μL of the internal standard cocktails and 5 mL of methanol:chloroform:formic acid (10:10:1) with sufficient mixing, and then placed at − 20 °C overnight, after repeated freezing through liquid nitrogen frozen and thawing through a thermostat water bath for five times. After overnight incubation, the sample was added with 2 mL Hajra's solution containing 0.2 M phosphoric acid and 1 M KCl, vortexed, and centrifuged for 5 min at 3000 rpm. The bottom organic layer of three layers with lipids was transferred to a new glass tube for each extract and concentrated under nitrogen until 200 μL. The mixture of each sample with a phase (isopropyl alcohol:hexane:100 mM ammonium acetate, 58:40:2) to 1 mL was transferred to a new tube rapidly and centrifuged at 14,000 rpm, 4 °C, for 20 min, of which 400 μL was transferred to a sample bottle test and loaded to a LC-MS system. The normal-phase silica liquid chromatography-coupled (NPLC) triple quadrupole mass spectrometer (QTRAP® 6500, SCIEX, Framingham, MA, USA) was used, and the Q-Trap was run in multireaction monitoring (MRM) mode. Precursor ion (PI) scans in the negative ion mode and neutral loss (NL) scans in the positive ion mode by electrospray

ionization mass spectrometry were applied to detect the ion pairs and obtained data (Han and Gross 2005). Every experiment was measured in triplicates.

Digitalization of clinical phenomes

Clinical phenomes of patients with lung cancer were digitalized and scored on the basis of the severity of phenomes, including clinical symptoms, physical examination, disease history, lung cancer grade, and laboratory tests for a total of 75 items. The scores of disease severities were divided into four levels: 0 for normal/none, 1 for mild, 2 for moderate, and 4 for severe. Family history without lung cancer was recorded as 0 and the one with lung cancer as 4. Based on the duration of the history of chronic obstructive pulmonary disease (COPD), patients without COPD history were scored as 0, within 5 years of COPD as 1, between 5 and 10 years of COPD as 2, and more than 10 years as 4. The normal range of biochemical measurements was scored as in Table 1, according to the extent beyond the normal range. The grade of lung cancer was evaluated on the basis of the condition of the primary tumor and lymph nodes as well as the appearance of distant metastases. The digital evaluation score system of patients with lung cancer was applied for various diseases (Wang et al. 2015; Xu et al. 2017).

Analysis of lipidomic profiles and integration with clinical phenomes

Lipids were identified using mass spectrometry and quantified in comparison to the internal standard, and lipidomic data were analyzed with the bioinformatics tool (Lipid MS Predict, http://www.lipidmaps.org). The data obtained by mass spectrometry was processed with MultiQuant™ software (AB Sciex), and the peak area of each pair was used for further quantification. The special-type lipids were identified as the fold change > 2 and p value < 0.05, as compared with other lung cancer subtypes. The co-expression of lung cancer lipids was identified as changes of lipid species in all lung cancers, fold change > 2, and p value < 0.05, as compared with healthy controls. The trans-points between lipidomic profiles and clinical phenomes were evaluated by the expression quantitative trait locus (*eQTL*) model.

Screening of targeted lipid-sensitive cells

The selected lipid elements contain fatty acid chains of lengths 16 and 18 without double bonds. The C16:0 and C18:0 were selected as the targeted lipids after analyses of plasma lipidomic profiles of patients with lung cancer. The sensitive lung cancer cells to C16:0 or C18:0 were further evaluated from human lung cancer cell lines, including large cell lung cancer cells (NCI-H460 and NCI-H661) expressing easily detectable p53 mRNA, small cell lung cancer cells (NCI-H1688), lung adenocarcinoma (NCI-H1650), nonsmall cell lung cancer cells (NCI-H1299), HPV-16 E6/E7 transformed normal bronchial epithelia (HBE135-E6E7), lung alveolar adenocarcinoma epithelia ($A549^{p53+}$), or lung bronchial adenocarcinoma epithelia (SPC-A1 cells). Cells were exposed to targeted lipids at different concentrations for different durations, respectively, in RMPI 1640 (KeyGEN, China) with penicillin 100 U/mL, streptomycin 100 mg/mL, and 10% fetal bovine serum (Corning Cellgro, Australia), at 37 °C in 5% carbon dioxide.

Measurement of cell proliferations

Cell proliferation was incubated in 90% RPMI 1640 for 2 h at 37 °C and then measured with 10% CCK-8 solution (Dojindo, Japan). Detection of OD value at 450 nm was done using FlexStation 3 multimode microplate reader (Molecular Devices, USA). All experiments were repeated at least six times. A549 or NCI-H1688 was selected as the sensitive cells to C16:0 or C18:0, respectively, and then seeded in 96-well plates with 2000 cells per well and exposed to C16:0 and C18:0 in concentrations of 0, 50, 100, or 200 μM for 24 or 48 h, respectively.

Target gene screening and validation

RNAs were extracted from the sensitive cells, washed with phosphate buffered saline, and added with 500 μL of TRIzol reagent (Invitrogen, USA) per well and 200 μL chloroform. mRNA of the target genes was amplified with quantitative real-time PCR with SYBR green fluorescence (Takara, Japan), after reversed transcription using PrimeScript RT Master Mix (Takara, Japan). Quantitative RT-PCR was implemented by ABI 7000 PCR instrument (Eppendorf, Hamburg, Germany), using two-stage program parameters. The process includes incubation at 95 °C for 2 min and 39 cycles

Table 1 Lung cancer bioinformatics

Variables	Points			
Clinical situation	0	1	2	4
Cough	No	Slight	Moderate	Severe
Sputum	No	Slight	Moderate	Severe
Hemoptysis	No	Rarely (blood in sputum)	Occasionally	Often
Dyspnea	No	After exercise	At ordinally living	At rest
Hoarse sound	No	Slight	Moderate	Severe
Fatigue	No	Slight	Moderate	Severe
Appetite	Good	Slight anorexy	Moderate anorexy	Severe anorexy
Sleep	Well	Slight anypnia	Moderate anypnia	Moderate anypnia
Anxiety	No	Slight	Moderate	Severe
Pain	No	Slight	Moderate	Severe (need pain-stopping pills)
Urination and defecation	Normal	Slight inconvenience	Moderate inconvenience	Severe inconvenience
PS score	0~1	2	3	4
Physical Examination	0	1	2	4
Mind	Clear	Drowsiness	Clouding of consciousness	Coma
Fever	Normal	37.3–38.0 °C	> 38.0–39.0 °C	> 39 °C
Heart rate	60–100/bpm			< 60 or > 100/bpm
Respiratory rate	16–20			> 20
Blood pressure (mmHg)	< 140/90	140–159/90–99	160–179/100–109	≥ 180/≥ 110
Weight loss (compare with former)	No	0–5%	5–10%	> 10%
Superficial lymph node	No	One site	Two sites	Multisites
Chest inspection	Normal			Positive sign
Chest palpation	Normal			Positive sign
Chest percussion	Normal			Positive sign
Chest auscultation (rale)	Normal			Positive sign
Heart	Normal			Positive sign
Abdomen	Normal			Positive sign
History	0	1	2	4
Lung cancer family history	No			Yes
COPD history	No	0–5 years	5–10 years	> 10 years
Lung TB history	No	0–5 years	5–10 years	> 10 years
Other lung disease history	No	0–5 years	5–10 years	> 10 years
Smoking (pack * year)	Never	0–20	21–40	> 40
Cancerogenic occupational environment	No	0–5 years	5–10 years	> 10 years
Other chronic disease history	No	0–5 years	5–10 years	> 10 years
Lung cancer stage (CT) (according to UICC TNM 2009)	0	1	2	4
T (tumor)	Tx and T1	T2	T3	T4
Sum of all T (mm)	0–30 mm (within 1/2 lobe for diffuse cancer)	31–50 mm (within 1 lobe for diffuse cancer)	51–70 mm (within 2 lobes for diffuse cancer)	> 70 mm (> 2 lobes for diffuse cancer)

Table 1 (continued)

Variables	Points			
Clinical situation	0	1	2	4
Onset of new lesion (T)	No			Yes
N (lymph node)	No	N1	N2	N3
Sum of all N (mm)	0	1–30 mm	30–60 mm	> 60 mm
Onset of new lesion (N)	No			Yes
Metastasis (pleural effusion)	No	Below 4th anterior rib	Between 2 and 4 anterior rib	Above 2nd anterior rib
Metastasis (contralateral lung)	No	Single lesion	2 lesions	Multilesions
Metastasis (brain)	No	Single lesion	2 lesions	Multilesions
Metastasis (bone)	No	Single lesion	2 lesions	Multilesions
Metastasis (adrenal gland)	No	Single lesion	2 lesions	Multilesions
Metastasis (other)	No	Single lesion	2 lesions	Multilesions
Onset of new lesion (metastasis)	No			Yes
Stage	I	II	III	IV
Laboratory examination (ULN = upper limit of normal; LLN = low limit of normal)	0	1	2	4
Hemoglobin (g/L)	Male 160–120 Female 150–110	Male 90–119 Female 90–109	60–89	≤ 59
Leukocytes (total WBC)	≥ 4.0×10^9/L	3.9–3.0×10^9/L	2.9–2.0×10^9/L	< 2.0×10^9/L
Neutrophils	≥ 2.0×10^9/L	1.9–1.5×10^9/L	1.4–1.0×10^9/L	< 1.0×10^9/L
Platelets (× 10^9/L)	≥ 100×10^9/L	99–75.0×10^9/L	74.0–50.0×10^9/L	< 50.0×10^9/L
Serum albumin (g/L)	≥ 35	34–30	29–25	< 25
ALT	Normal	>ULN–2.5 × ULN	>2.5–5.0 × ULN	> 5.0 × ULN
AST	Normal	>ULN–2.5 × ULN	>2.5–5.0 × ULN	> 5.0 × ULN
Bilirubin	Normal	>ULN–1.5 × ULN	>1.5–3.0 × ULN	> 3.0 × ULN
Direct bilirubin	Normal	>ULN–1.5 × ULN	>1.5–3.0 × ULN	> 3.0 × ULN
Urea (mmol/L)	3.2–7.1	7.2–9.0	9.1–19.9	> 20
Creatinine (μmol/L)	40–115	116–178	179–445	> 445
Uric acid	Normal			
Na (mmol/L)	136–145	146–150 or 135–130	151–155 or 131–125	> 155 or < 125
K (mmol/L)	3.5–5.2	3.0–3.4 or 5.3–5.5	2.5–2.9 or 5.6–6.0	< 2.5 or > 6.0
Cl (mmol/L)	96–105			> 105 or < 96
Ca (mmol/L)	2.15–2.55	> 2.55–2.90 or < 2.15–2.0	> 2.9–3.1 or < 2.0–1.75	> 3.1–3.4 or < 1.75–1.5
P (mmol/L)	0.9–1.34			> 1.34 or < 0.9
PH	7.35–7.45	7.35–7.30	7.25–7.30	< 7.25
PaO_2 (mmHg)	≥ 90	70–89	60–69	< 60
$PaCO_2$ (mmHg)	35–44	45–47	48–50	> 50
SCC	Normal	> 1 × ULN	> 2 × ULN	> 3 × ULN
CEA	Normal	> 1 × ULN	> 2 × ULN	> 3 × ULN
Cyfra211	Normal	> 1 × ULN	> 2 × ULN	> 3 × ULN
CA125	Normal	> 1 × ULN	> 2 × ULN	> 3 × ULN
NSE	Normal	> 1 × ULN	> 2 × ULN	> 3 × ULN
CRP	Normal	> 1 × ULN	> 2 × ULN	> 3 × ULN

Table 1 (continued)

Variables	Points			
Clinical situation	0	1	2	4
PT (s)	10.0–13.0	13.1–16		> 16
Free blood glucose (mmol/L)	3.9–6.9	7.0–8.9 or 3.0–3.8	9.0–13.9 or 2.5–2.9	> 14.0 or 2.0–2.4
Sum of all				

for 5 s at 95 °C and 30 s at 60 °C. Sequences of the primers were human ACSL5, (reverse) 5′-CGTC AGCCAGCAACCGAATATCC-3′ and (forward) 5′-GTCATCTGCTTCACCAGTGG-3′; human CSF2: (reverse) 5′-CAGGAAGTTTCCGGGGTTGG-3′ and (forward) 5′-GCCCTGGGAGCATGTGAATG-3′; and human β-actin: (forward) 5′-AGCGAGCATCCCCC AAAGTT-3′ and (reverse) 5′-GGGCACGAAGGCTC ATCATT-3′. After normalization of internal control (β-actin), the relative mRNA expression level is evaluated by calculating $2^{(-\Delta\Delta Ct)}$ values based on the threshold cycle (Ct) values. The measurement was at least repeated three times per group.

Dynamic measurements of cell biobehaviors

The live-cell imaging technology Cell-IQ (Chip-Man Technologies, Tampere, Finland) was utilized to record cell number, proliferation, division, death, apoptosis, and movement of tumor cells, with a phase contrast microscope (Nikon CFI Achromat phase contrast objective with 910 magnifications) and a camera (Nikon, Fukasawa, Japan), to obtain continuous dynamic cell information and to take pictures every 2 h until 72 h. The Cell-IQ was operated by adopting the Manual Tracking plug-in produced by Fabrice Cordelieres (Institut Curie, Orsay, France) and getting data through a freely distributed image software (Cell-IQ Imagen v2.9.5c; McMaster Biophotonics Facility, Hamilton, ON, Canada). The machine vision technology of Cell-IQ can get sufficient evidence of high quality and quantitative changes to analyze cell function and morphological parameters. About 12 images of each single cell were taken and collected at each time point.

RNA interference

Three different sequences of ACSL5 or CSF2 siRNA were designed and synthesized (GenePharma, Shanghai, China), as follows: ACSL5-Homo-731: GCUUGUUACACGUACUCUATT, UAGAGUACGUGUAACAAGCTT; ACSL5-Homo-1509: GCGGAAGGGUUCGUGUAAUTT, AUUACACGAACCCUUCCGCTT; ACSL5-Homo-1604: GCUUAUGGUCAAACAGAAUTT, AUUCUGUUUGACCAUAAGCTT; CSF2-Homo-157: CUGAACCUGAGUAGAGACATT, UGUCUCUACUCAGGUUCAGTT; CSF2-Homo-202: GAAGUCAUCUCAGAAAUGUTT, ACAUUUCUGAGAUGACUUCTT; CSF2-Homo-370: GCAACCCAGAUUAUCACCUTT, AGGUGAUAAUCUGGGUUGCTT), NC (negative control: 5-UUCUCCGAACGUGUCACGUTT-3, 5-ACGUGACACGUUCGGAGAATT-3), and Lipofectamine 2000 (Invitrogen). Lipofectamine 2000 was added per microliter to NC or siRNA per 20 pmol/well for 20 min at room temperature. After 24 h of interference at 37 °C, the expression of mRNA was detected using real-time-PCR to assess the effectiveness of the interference. ACSL5-Homo-731 and CSF2-Homo-202 were screened as effective sequences of stable transfection of ACSL5 and CSF2 genes and further experiments were conducted.

Cell cycle detection

Cell cycle and division of A549 and H1688 were measured using the Cell Cycle Detection Kit (KeyGEN Biotech, China), respectively. Cells were plated on a six-hole plate and cultured for 24 h. After interfering with the gene, the cells were collected after stimulation with C16:0 and C18:0 200 μM for 6, 12, and 24 h. Each sample was washed with PBS and centrifuged for 5 min 2000 rpm, fixed with 10% formalin fixative solution 500 μL for 10 min, and washed with PBS. Every sample was added with 500 μL working solution according to 1:9 volume configurations of RNase A:propidium iodide (PI). The sample was analyzed with a Flow

Cytometer (BD FACSAria II, USA) using FlowJo 7.4 version (FlowJo software, USA).

ATP detection

Cells were cultured in the 6-well plate for 24 h and interfered with the gene and lipid stimulation for 24 h, and then digested; 10,000 cells per well were transferred into the 96-well plate. After cells were completely attached using ATPlite step purchase from PerkinElmer (USA, 6016736), 100 μL reconstituted reagent was added to each well. The ATP standard solution with four gradients are established and the 96-well microplate was then shaken for 2 min for the measurement of luminescence.

Flow fluorescence detection

After cells are cultured in a 6-well plate, lipid stimulation, gene interference, and post-interference lipid stimulation were performed, respectively, at different time points. The Mito Tracker™ Green FM (Invitrogen, OR, USA) and Mito Tracker™ Red (Invitrogen, OR, USA) were added and then incubated for 20 min at 37 °C. Carnitine palmitoyl transferase 1A (CPT1A) (Proteintech, Chicago, USA) was incubated for 30 min and transferred into the flow tube for Flow Cytometer (BD FACSAria II, USA) after completion.

Statistics

Data were presented as mean ± SE. One-way ANOVA was used for statistical differences between different groups, and Student's *t* test with one way and two-tailed was used for differences between two groups. The statistical difference for each lipid species is calculated by fold change and *p* value based on the average of each lung cancer subtype and healthy control. Volcanic maps of different lung cancer subtypes and healthy controls based on mass spectrometry data were made using MetaboAnalyst, based on the absolute value of log 2 (fold change) of 1 and p value < 0.05. To assess the correlation between clinical scores and lipid species, this was achieved by simulating the *eQTL* model. MatrixEQTL R package was used to obtain the degree of correlation and *p* value between the score and the lipid. When comparing different lung cancer groups, we obtained the group-specific score–lipid pairs p value < 0.05. MatrixEQTL implements additive linear models with additive and dominant effects. The Cell-IQ statistical method is as follows: rate (%) = value at each time point value of primary seeding cells / mean value of primary seeding cells. According to the KEGG annotation results and classification, the biological pathways with statistically different genes are classified, and the KEGG metabolic pathways involved in the genes are divided into six branches. Flow fluorescence data analysis was conducted using FlowJo 7.6 version.

Results

Understanding of patient phenomes

Clinical phenomes of patients with lung cancer are scored and listed in Supplemental Table 1. About 19% of patients with lung cancer were at Tx/T1 of tumor staging, 27% in T2, 15% in T3, and 38% in T4, of which ADC and SCC tumor staging were higher. Some patients with ADC had distant metastases of primary cancer, e.g., contralateral lung, brain, bone, or liver, rather than other patients. Lipidomic profiles demonstrated that the highest level of PS34:4 was noticed in patients with ADC, as compared with other subtypes of lung cancer, and patients with lung cancer had a low level of d17:1So, especially in ADC. Patients with a lower level of d17:1So may have less metastatic rate. Lung cancer co-regulated lipidomic profiles is listed in Table 2, where the levels of lysoPC20:3, PC32:2, or PC33:2e were significantly lower in lung cancer and the lowest in ADC patients.

Lipidomic profiles of patients with lung cancer

On the basis of comprehensive information on qualitative and quantitative analyses of lipid composition, 385 unique lipids were detected in healthy individuals and patients with subtypes of lung cancer through neutral loss in positive or precursor ion scanning in negative mode electrospray ionization tandem mass spectrometry. The number of 12 major detection subclasses of lipids is classified and shown in Fig. 2a, where the proportion of response intensity of lipids was shown in total measurement (Fig. 2a(1)), healthy control (Fig. 2a(2)), SCC (Fig. 2a(3)), ADC (Fig. 2a(4)), or SCLC (Fig. 2a(5)). It was found that some lipid elements

Table 2 Co-expression of lipids in plasma over twofolds in adenocarcinoma (ADC), squamous cell carcinoma (SCC), or small cell lung cancer (SCLC)

Lipid name	ADC fold	SCLC fold	SCC fold
Fold change > 2, $p < 0.05$			
Cer24:0	2.862307	2.646822	2.584011
Cer25:0	4.593269	3.410717	4.675704
lysoPE14:0	6.075508	4.509418	4.476154
PE36:5	3.476027	4.307447	4.740026
PE38:7	13.88299	19.55051	11.60443
Fold change < 0.5, $p < 0.05$			
d17:1So	0.033062	0.22666	0.448922
d18:1So	0.018086	0.012112	0.03311
lysoPC18:2	0.466565	0.328987	0.406365
lysoPC20:3	0.2842	0.388031	0.386161
lysoPC20:4	0.167714	0.165871	0.187154
lysoPC22:4	0.04893	0.038327	0.056135
lysoPC22:6	0.303424	0.221405	0.322331
lysoPE18:2	0.262675	0.308689	0.465309
lysoPE20:3	0.087032	0.038238	0.144453
lysoPE20:4	0.040011	0.034344	0.111629
lysoPE20:5	0.265641	0.149567	0.084688
lysoPE22:6	0.085642	0.110134	0.159334
lysoPI20:4	0.213547	0.472123	0.310416
lysoPI22:0	0.19909	0.342175	0.269218
PC32:2	0.330958	0.365122	0.457137
PC33:2e	0.357246	0.416174	0.381441
PE33:1	0.146865	0.141788	0.350503
PE33:2	0.113344	0.151211	0.400366
PE35:2	0.371418	0.454159	0.494954
PE35:3	0.242469	0.212768	0.374656
PE35:4p	0.151477	0.2012	0.389858
PE37:4	0.203804	0.229325	0.353764
PE39:6	0.274575	0.302664	0.474979
PI36:6	0.226573	0.498263	0.243319

increased in patients with lung cancer, e.g., PE36:5, PE38:7, Cer24:1, Cer24:0, and Cer25:0 co-upregulated in each disease group in Fig. 2b. The distribution of upregulation and downregulation of lipids varied among the groups of SCC, ADC, or SCLC and is shown in the volcano plot (Fig. 2c(1), c(2), or c(3), respectively). Levels of downregulated and upregulated lipid molecules more than twofolds with statistical significance were scattered in the upper left and upper right distributions, respectively.

Figure 2d demonstrates changes of some lipid species classified by the number of C atoms among subtypes of lung cancer. Levels of C16:0 and C16:1 were lower in patients with lung cancer, while levels of C18:0, C20:2, C20:3, C20:4, or C22:6 were significantly higher in patients with ADC, SCC, or SCLC. Levels of 18:1 and 18:2 were lower in SCC than those in healthy controls or patients with ADC or SCLC. Downregulated palmitic acid (16:0) and upregulated stearic acid (18:0) were selected as target lipid elements for further validation. PC, LPC, and PG accounted for the major portion. Levels of PG, LPC, LPE, and lysophosphatidylglycerol (LPG) were significantly lower in patients with lung cancer, as compared with the healthy controls. In addition, the levels of PG were significantly lower in ADC, LPC in ADC and SCLC, or LPG and lysophosphatidylinositol (LPI) in SCC, respectively, while the levels of LPS were significantly higher in SCC and ADC, as compared with the healthy controls (Fig. 2e).

Trans-omics points between lipidomic profiles and clinical phenomes

The trans-points between the changes of lipid molecules in plasma and major clinical phenomes of patients with ADC, SCC, or SCLC were analyzed by simulating the *eQTL* model and detailed in Supplemental Table 2. In addition, after comparing all statistically significant lipid species we have calculated with simulated *eQTL* analysis methods, we have obtained a heat map of trans-points between lipid species and clinical phenomes (Fig. 3). Lipidomic profiles and clinical phenomes from all patients with lung cancers were pooled together for the detection of trans-points (Fig. 3a), where two fatty acid chain lengths of C16 and C18 appeared significant in most of the patients. The grade of tumor development and the onset of new lesion were of the highest correlation with lipids in patients with SCC, and there were 49 trans-points crossing between lipids and phenomes (Fig. 3b). High expression of carcinoembryonic antigen (CEA) was associated with 10 lipid molecules, namely lysoPS22:6, lysoPS18:2, Cer24:0, lysoPS18:1, lysoPS20:2, lysoPS22:4, lysoPS20:3, lysoPS22:0, d17:1So, and Cer25:0 in patients with ADC (Fig. 3c). Fever, COPD history, and hemoptysis were crossed with d17:1S1P, Cer12:0, or Cer25:0 in SCLC patients (Fig. 3d). A clinical phenome can correspond to a

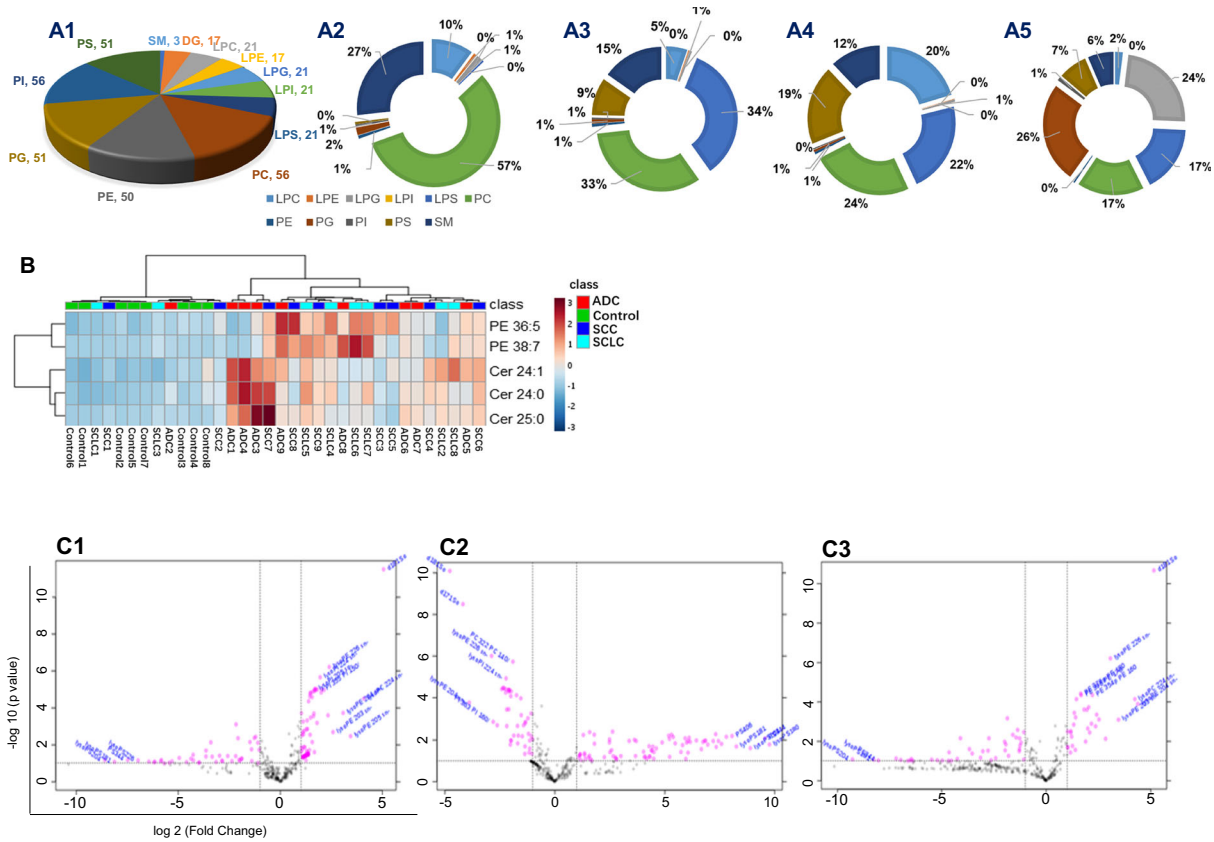

Fig. 2 Lipidomic profiles among patients with lung squamous cell carcinoma (SCC), lung adenocarcinoma (ADC), or small cell lung cancer (SCLC). **a** (1) The number of lipid subclasses in the lipid detection list. For example, DG detects 17 lipid species, LPC detects 21 lipid species, and all 12 lipid categories detect a total of 385 lipid species. **a** (2) The response intensity of the 11 lipid subclasses in the control group as a percentage of the total. **a** (3) The SCC response intensity ratio. **a** (4) ADC and **a** (5) SCLC. Heat map (**b**) indicates the distribution of five lipid molecules co-upregulated in three subtypes of lung cancer in each patient. **c** The transverse axis of the volcano map represents fold change, the longitudinal axis stands for *p* value, and the points at the upper left and upper right represent lipid molecules that are downregulated and upregulated by more than twofolds compared with healthy people, respectively. **c** (1) For SCC, **c** (2) for ADC, and **c** (3) for SCLC ($p < 0.05$). **d** C atom distribution map. In this diagram, we can figure out that the C16, C18, and C20 fatty acyl chains are mainly distributed in lipid series. Moreover, the expression of C16:0, C16:1, and C18:2 in lung cancer patients was lower than that in normal controls and was more obvious in patients with SCC than in patients with SCLC, while C18:0 and C20:4 were upregulated in three types of lung cancer (one-way ANOVA *, **, and *** stand for $p < 0.05$, 0.01, and 0.001). **e** Different kinds of lipid subclasses. It was found that PC, LPC, and PG accounted for important parts among them. In many kinds of lipids, the decrease of PG, LPC, LPE, and LPG in the three types of lung cancer was more obvious than that in normal persons. Among them, LPC has the highest response intensity, which has more significance

variety of lipid elements, while a lipid element was also crossed with many clinical phenomes. For example, PS38:6 was trans-pointed with seven clinical phenomes in ADC patients.

Screening of target lipid-sensitive cells and biological behaviors

C16:0 and C18:0 were selected as target lipids to screen target lipid-sensitive lung cancer cells, on the basis of the results from mass spectrometry that most of the selected lipid molecules contained fatty acids with lengths of 16 and 18 without double bonds. Of HBE, A549, H460, H1299, H661, H1688, H1650, and SPC-A1, C16:0 or C18:0 significantly inhibited the proliferation of HBE, A549, and H1650 (Fig. 4a) or HBE, H1688, and H1650 (Fig. 4b) in a dose-dependent pattern ($p < 0.05$ or less, respectively). Of those cells, A549 cells were more sensitive to C16:0 (Fig. 4) and H1688 cells to C18:0 (Fig. 4b). Dynamic proliferation,

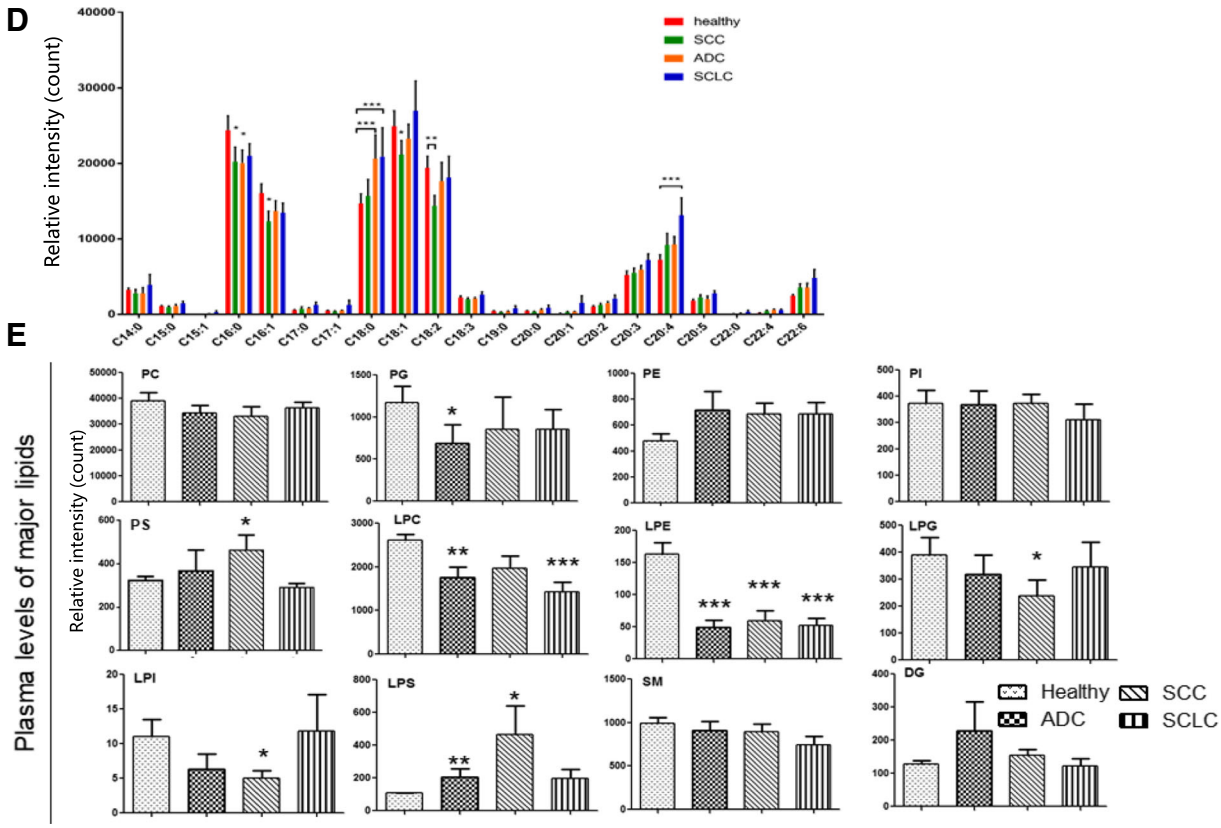

Fig. 2 (continued)

differentiation, death, and movement of A549 (Fig. 4c) and H1688 cells (Fig. 4d) were monitored during 72 h after cells were treated with C16:0 and C18:0, respectively. C16:0 or C18:0 could inhibit the dynamic proliferation of A549 or H1688 cells, while it increased the number of dead cells gradually after the treatment (Fig. 4c, d). There was no significant difference in cell differentiation and movement of A549 or H1688 treated with vehicle or target lipids.

Transcriptional profiles of target lipid-sensitive cells

In order to identify target lipid-associated transcriptional profiles and potential signal pathways, we defined the patterns of up- or downregulated genes and changes of functional clusters in A549 (Fig. 5a, c) or H1688 cells (Fig. 5b, d) 24 and 48 h after treatment with C16:0 or C18:0 at concentrations of 50, 100, or 200 μM, respectively. The number of up- or downregulated expression genes of both cells with lipid elements increased or decreased in a dose- or time-dependent pattern. The number of upregulated genes in A549 was consistently higher than that of downregulated genes during different times with various doses of C16:0, while such increase in H1688 was noticed at 100 and 200 μM of C18:0 in 24 h and 50 μM in 48 h. The number of changed genes in H1688 cells was obviously higher than that in A549 cells. During bioinformatics analyses of functional clusters, alterations of functional patterns were compared among cells with or without target lipids, cells with different doses of target lipids, cells at different time points, and different cells. Data focusing on cellular processes, environmental information processing, genetic information processing human disease metabolism, and organismal systems are presented in Fig. 5c and d. In those five focused areas, major changes of functional cluster varied between A549 and H1688, e.g., cellular communication, transcription, infectious diseases viral and parasitic, immune system, and excretory system in A549, while transport and catabolism, replication and repair, cancer special types, drug resistance antineoplastic, endocrine system, or aging in H1688, when each functional cluster was compared. Of those five focused areas, major variations were observed

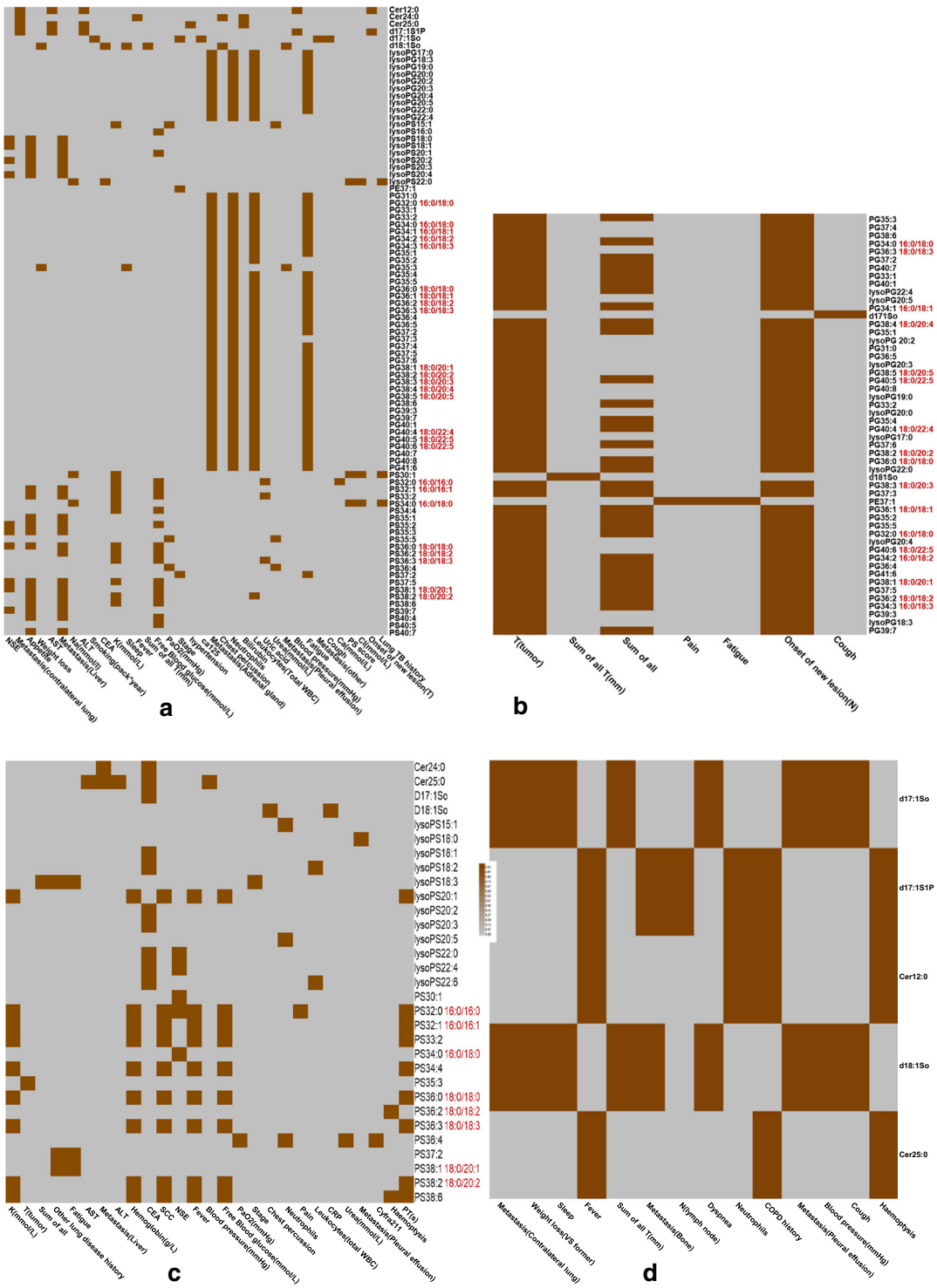

Fig. 3 Clinical lipidomics by integrating lipidomic profiles with clinical phenomes. By simulating the expression quantitative trait locus (*eQTL*) model, we obtained the heat map of the correlation between clinical symptom and lipid specie. The abscissa is the related clinical symptom, the ordinate is the corresponding lipid specie, and if the two are correlated, the color is brown and has statistical significance ($p < 0.05$). The red color indicates that this lipid specie has 16 or 18 C atoms in the main chain. **a** The correlation heat map of all lung cancer patients with clinical phenotype. **b** SCC group. **c** ADC group. **d** SCLC group. In the heat map, brown indicates that the two are related, and gray indicates that they are not related

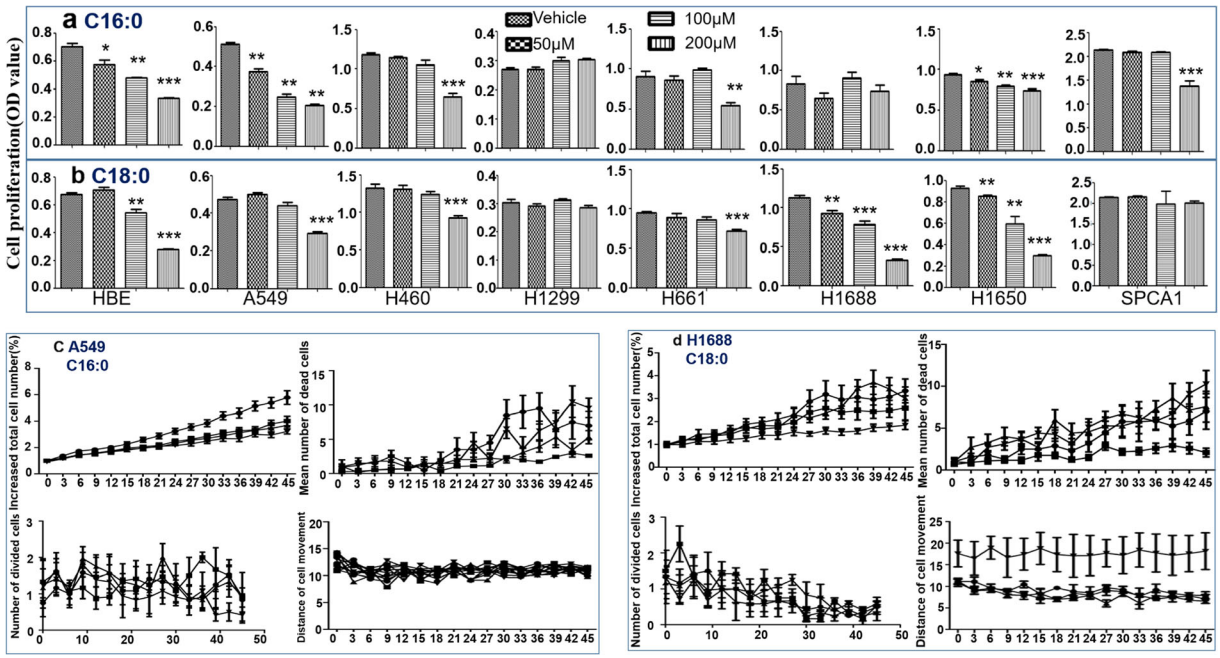

Fig. 4 Identification and validation of target lipid-sensitive lung cancer cells. **a** C16:0 and **b** C18:0 act on nine types of lung cancer cells including HBE135-E6E7, A549^{p53+}, NCI-H460, NCI-H1299, NCI-H661, NCI-H1688, NCI-H1650, and SPC-A1. It was found that the inhibitory effect of C16:0 on A549 or C18:0 on H1688 was the most obvious, when C16:0 and C18:0 were treated in three different doses. **c**, **d** These figures showed dynamic alterations of the A549 and H1688 cells stimulated with C16:0 and C18:0 of A549 (**c**) and H1688 (**d**) after treated with C16:0 and C18:0 50, 100, and 200 μM compared with vehicle. H1299 cells are not sensitive to both lipid stimulations. The number of dead cells was higher after C16:0 and C18:0 treated. The mean number of divided C16:0-treated A549 cells and C18:0-treated H1688 cells shows no obvious change compared with vehicle, and the ability of movement did not change significantly

between A549 (Fig. 5c) and H1688 (Fig. 5d) in the area of metabolism. Of the top 10 upregulated genes of A549 cells at 24 h (Fig. 5e) and 48 h (Fig. 5f) or H1688 cells at 24 h (Fig. 5g) and 48 h (Fig. 5h) after treatment with C16:0 or C18:0 at 50, 100, or 200 μM, the expression of ACSL5 or CSF2 genes significantly increased in A549 or H1688, in a dose-dependent and time-dependent manner, and they were selected as the target lipid-associated genes for A549 or H1688, respectively.

Validation of target lipid-associated gene functions

The target lipid-associated genes selected from RNA-Seq in sensitive cells were further validated and the treatment with C16:0 or C18:0 increased the expressions of ACSL5 or CSF2 genes in A549 (Fig. 6a) or H1688 cells (Fig. 6b) in time- and dose-dependent patterns ($p < 0.05$ or less, respectively). The expression of C-C motif chemokine ligand 3 (CCL3) and pyruvate dehydrogenase kinase 4 (PDK4) was further investigated in order to understand potential involvements of those genes related to the regulation of target lipid-associated genes. C18:0 increased CCL3 expression in a time- and dose-dependent pattern (Fig. 6c, $p < 0.01$), while PDK4 expression reduced from 50 μM at 24 h and significantly increased at 48 h (Fig. 6d, $p < 0.05$). C16:0 increased PDK4 expression with an increase of doses and time and reached statistical significance in 100 μM at 24 h and 50 μM at 48 h (Supplemental Fig. 1, $p < 0.01$ or 0.05, respectively).

After screening of siRNA sequencing, the inhibitory effects of ACSL5 siRNA (Fig. 6e) or CSF2 siRNA (Fig. 6f) were evaluated to select the proper dose of siRNA for further validation. A549^{ACSL5-} cells had a similar capacity of proliferation to A549^{ACSL5+} when treated with vehicle (Fig. 6g). Compared with A549^{ACSL5+} cells, the proliferation inhibition of A549^{ACSL5-} cells reduced to a certain extent after C16:0 treatment. The proliferation of H1688^{CSF2+} cells treated with C18:0 was significantly lower than that with vehicle. Similarly, the effect of H1688^{CSF2-} on the inhibition of cell proliferation after C18:0 is reduced, and there is a tendency to

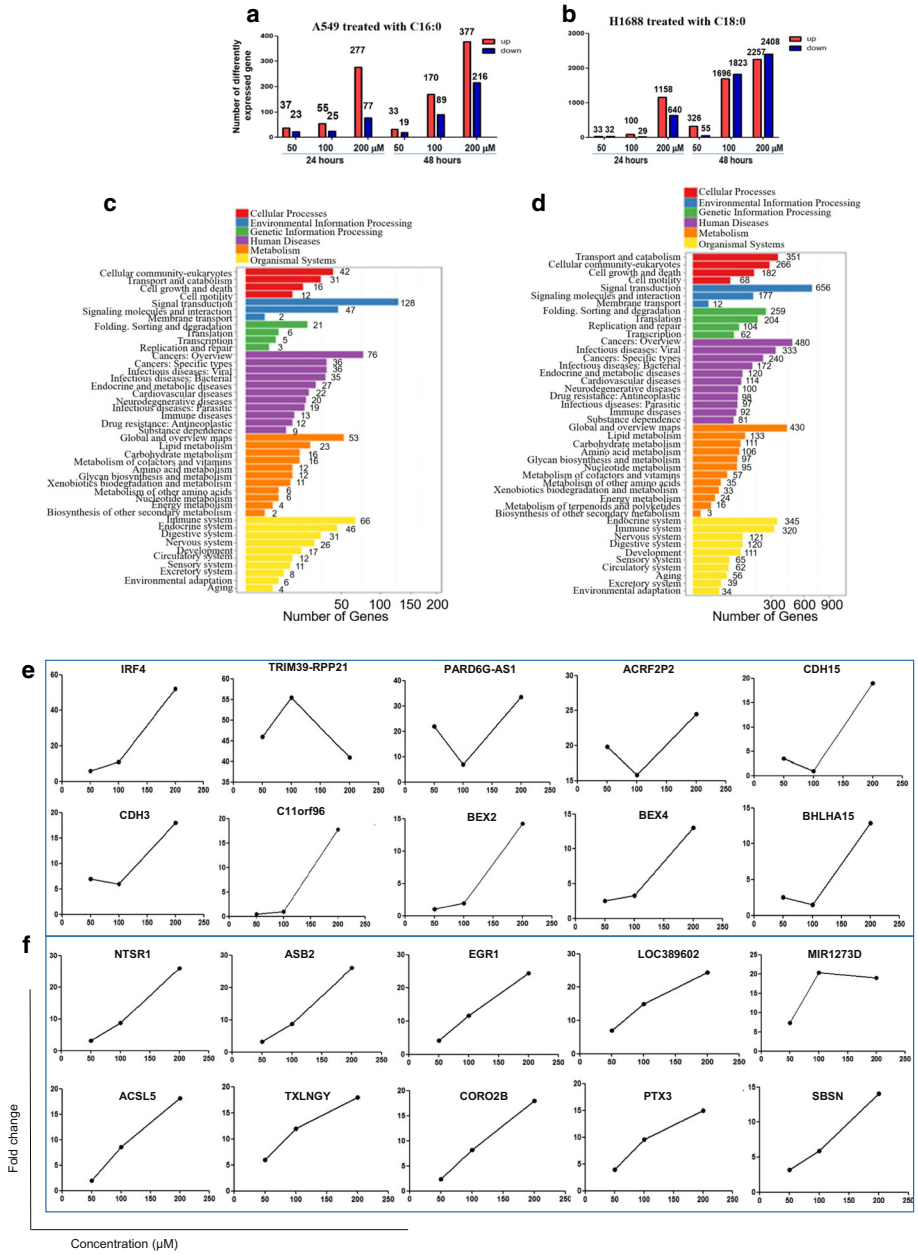

Fig. 5 Transcriptional profiles of target lipid-sensitive cells and molecular mechanisms. **a**, **b** The RNA-Seq of A549 and NCI-H1688 after treated with C16:0 or C18:0 at different doses and times. From the diagram, we come to the conclusion that the number of specific gene expression were dose- and time-dependent. The clustering of the KEGG pathway can be seen from the effect of 200 μM lipid for 48 h, and the most metabolism association of genes is involved in lipid metabolism, carbohydrate metabolism, cofactors and vitamins, xenobiotics biodegradation and metabolism, or other amino acids, nucleotide, as well as energy biosynthesis of other secondary metabolism in A549 (**c**) and H1688 (**d**). In the results of RNA-Seq, of the top 10 upregulated genes of A549 cell at 24 h (E) and 48 h (F), the levels of ACSL5 expression significantly increased in A549 cells after treated with C16:0 from 50 to 200 μM at 48 h and in a concentration-dependent manner. There was no repeat of the first 10 upregulated genes in 24 and 48 h. Of the first 10 genes of C18:0 acting at 24 h (**g**) and 48 h (**h**) on H1688 cells, there was an overlapping gene CSF2. In these figures, the abscissa represents the concentrations of 50, 100, and 200 μM, and the ordinate represents the fold change compared to the vehicle

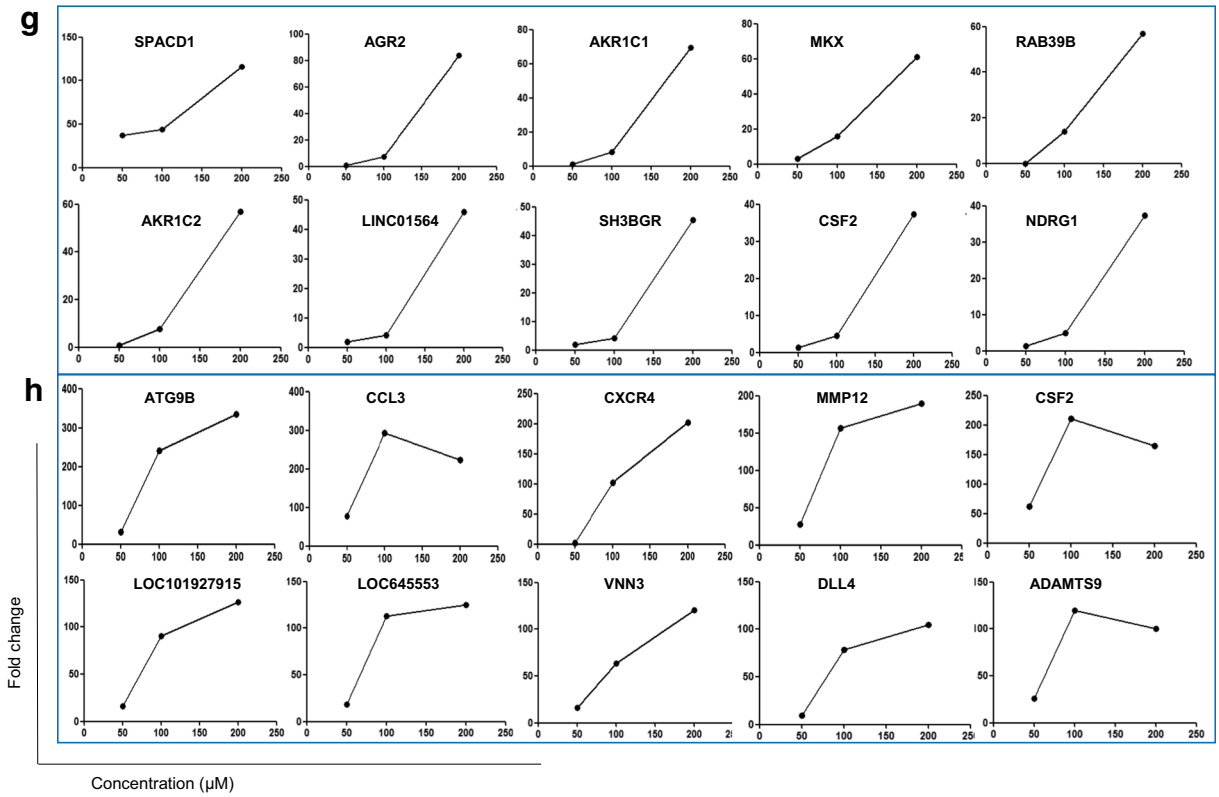

Fig. 5 (continued)

rise (Fig. 6h). In order to explore the effect of lipid on the cell cycle, the cell number in different phages (G1, G2, and synthesis) was counted 6, 12, and 24 h after treatment with C16:0 or C18:0 at 200 μM. The number of $A549^{ACSL5-}$ cells with vehicle in the G1 phase increased, and in the S phase, it reduced at 12 h. The treatment with C16: 0 significantly increased the number of $A549^{ACSL5+}$ cells in the S phase at 6 h, as compared with $A549^{ACSL5-}$ cells (Fig. 6i). In H1688 cells, the difference between $H1688^{CSF2+}$ and $H1688^{CSF2-}$ cells after C18:0 stimulation is more pronounced over time on the S phase (Fig. 6j).

There was no difference of the ATP content between $A549^{ACSL5+}$ and $A549^{ACSL5-}$ cells (Fig. 7a) or between $H1688^{CSF2+}$ and $H1688^{CSF2-}$ cells (Fig. 7b) treated with vehicle. The ATP content in $A549^{ACSL5-}$ cells was significantly lower than that in $A549^{ACSL5+}$ cells after treatment with C16:0 (Fig. 7a, $p < 0.05$), while in $H1688^{CSF2-}$ cells, it increased after treatment with C18:0 (Fig. 7b, $p < 0.05$). In order to further study the effect of lipid on mitochondrial function, the intracellular number of mitochondria and mitochondrial membrane potential were analyzed by Mito Tracker™ Green FM and Mito Tracker™ Red fluorescent dyes, respectively. The number of mitochondria in $A549^{ACSL5-}$ or $H1688^{CSF2-}$ cells was significantly higher than that in $A549^{ACSL5+}$ or $H1688^{CSF2+}$ cells after treatment with C16:0 (Fig. 7c, $p < 0.05$) or C18:0 (Fig. 7f, $p < 0.0001$), respectively. The value of mitochondrial membrane potential in $H1688^{CSF2-}$ cells was significantly higher than that in $H1688^{CSF2+}$ cells after treatment with C18:0 (Fig. 7g, $p < 0.05$). There was no difference of mitochondrial membrane potential between $A549^{ACSL5-}$ and $A549^{ACSL5+}$ cells (Fig. 7d). C16:0 reduced significantly the levels of long-chain fatty acid oxidation in $A549^{ACSL5-}$ cells, while not in $A549^{ACSL5+}$ cells (Fig. 7e). There was no obvious difference between $H1688^{CSF2-}$ and $H1688^{CSF2+}$ cells (Fig. 7h).

Discussion

The present study screened and identified lung cancer-specific, lung cancer subtype-specific, and clinical phenome-specific target lipid species using the principle of clinical trans-omics between clinical phenomics

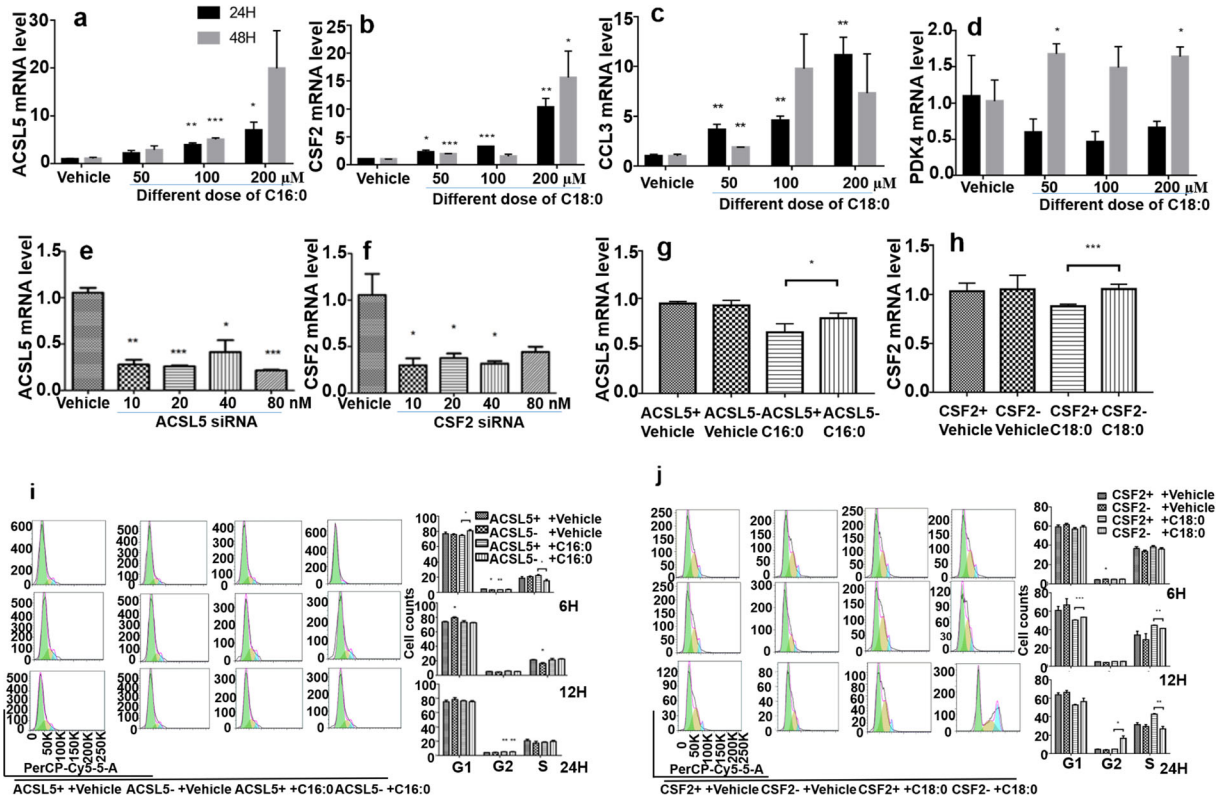

Fig. 6 Validations of target lipid-associated gene networks and target lipid-specific gene regulation. Four genes were screened from RNA-Seq results for 24 and 48 h validation. **a**–**d** PCR results verify for four genes. Expression of ACSL5 gene in A549 cells treated with C16:0 for 24 and 48 h (**a**). It can be seen that the gene expression increases with the increase of C16:0 concentration. After C18:0 acted on H1688 for 24 and 48 h, the expression of CSF2 increased more obviously (**b**), the expression of the other two genes, CCL3, also increased with increasing concentration, but in PDK4, the expression trends of 24 and 48 h were opposite (**c**, **d**). We selected the best effective interference concentration of ACSL5 siRNA-731 (**e**) and CSF2 siRNA-202 (**f**). Interference with A549 (**g**) and H1688 (**h**) inhibited these two kinds of cell proliferation treated with vehicle and prevented from cell proliferation after treatment with C16:0 and C18:0 at 200 μM for 24 h ($p < 0.05$ or less, respectively), respectively. **i** After interference with ACSL5, C16:0 200 μM was used to stimulate for 6, 12, and 24 h. **j** After interfering with CSF2 and C18:0 200 μM stimulation, compared with not interfering with CSF2 then C18:0 stimulation, the change of S phase is more and more obvious (* and ** stand for p values less than 0.05 and 0.01)

and lipidomic profiles (Zhang et al. 2020; Wang 2018). The previous study integrated clinical phenomics, lipidomics, and transcriptomics and found lung cancer-specific and lung cancer subtype-specific biomarkers on the basis of statistical analyses, multiple omics correlations, and significant difference (Lv et al. 2018a). In addition to lung cancer, disease-associated patterns of altered lipidomic profiles were found between infection- and noninfection-initiated acute lung injury and between primary infection and acute exacerbation of chronic lung disease (Gao et al. 2019). The present study furthermore focused on lung cancer subtype-specific trans-points/crossing-points between clinical phenomic and lipidomic networks to define an individual phenome corresponding to lipid(s) or lipid to phenome(s). Clinical phenomics is considered as a new emerging discipline not only for identifying disease-specific biomarkers, but also for discovering novel targets for the development of new therapies (Han et al. 2015). The new subphenotypes and subcategories of diseases can be identified by integrating clinical phenomes and molecular multiple omics (Zerin et al. 2015). The present study furthermore identified palmitic acids or stearic acids as target lipids in lung cancer and multiple trans-points between clinical phenomic and lipidomic profiles (Yugi et al. 2016).

Biomarkers of NSCLC and potential mechanism were identified through lipidomics (Chen et al. 2018),

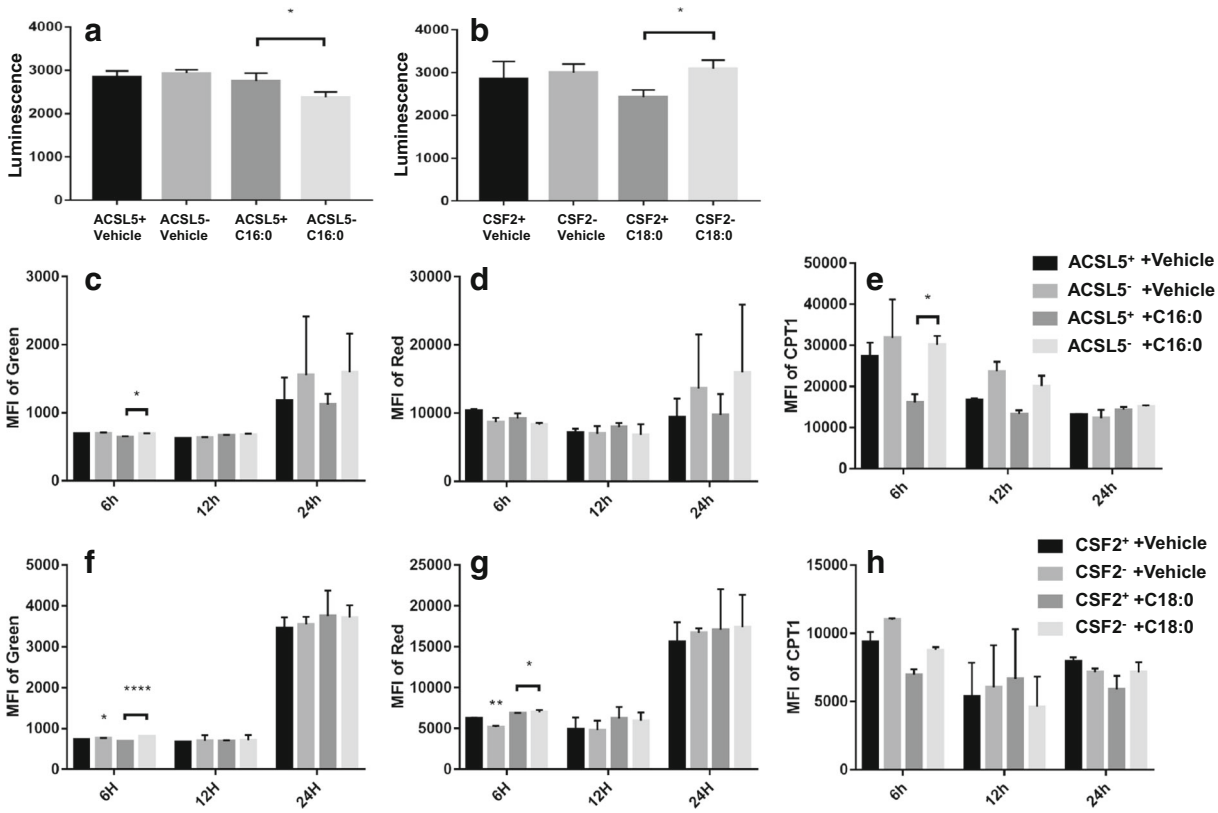

Fig. 7 Validations of target lipid-associated bioenergy production and mitochondrial function. **a** A549 and **b** H1688 cells were stimulated by C16:0 200 μM and C18:0 200 μM after interfering with ACSL5 and CSF2, respectively. The changes of ATP in the two kinds of cells were detected. **c**–**h** Flow cytometry was used to detect the mean fluorescence intensity (MFI) of Mito Tracker™ Green FM and Mito Tracker™ Red and CPT1. Among them, Mito Tracker™ Green is to detect the number and activity of mitochondria, and Mito Tracker™ Red is to detect mitochondrial membrane potential and CPT1 measuring fatty acid oxidation. **c**–**e** In the detection of Mito Tracker™ Green in A549 cells, it can be seen that after interfering with the gene and then stimulated with C16:0, the number of mitochondria is increase and more active (**c**), and the metabolism of fatty acids in CPT1 detection is also relatively enhanced (**e**). **f**–**h** In H1688 cells, there was a similar effect, and the increase in mitochondrial membrane potential was more pronounced (**g**). (*, **, and **** represent $p < 0.05$, 0.01, and 0.0001)

and human lung resident cells were used to understand the changes of lipid in lung diseases and lipid-involved pathological process of diseases (Zemski Berry et al. 2017). Using a panel of lung cancer cells with different molecular phenotypes corresponding to different subtypes of clinical categories, C16:0 or C18:0 was found to be antiproliferative and cells were divided into more sensitive cells to C16:0 (A549), to C18:0 (H1688), or to both (HBE, H1650), with time- and dose-dependent responses to target lipids. It is questioned whether the variation of C16:0 and C18:0 levels in the circulation may result from the difference of lipid metabolisms, production sources, organ/tissue consumptions, or interactions with lung cancer cells. Of those potentials, it seems that the interaction between target lipids and lung cancer cells is independent upon systemic levels of patients, which may be disease-associated biomarkers (Mirtavoos-Mahyari et al. 2019; Doumandji et al. 2019). Various responses of lung cancer cells to target lipids may be associated with genetic heterogeneity, although the exact mechanisms remain unclear. Target lipids could inhibit alterations in proliferation and death patterns of ADC and SCLC cells, rather than cell differentiation and movement.

To further explore novel mechanisms by which two target lipids may interact with the corresponding sensitive cells through different or similar pathways, transcriptional profiles of ADC or SCLC cells were studied by temporal gene expression analysis at different time points after treatment with C16:0 or C18:0, respectively. From functional clusters of transcriptional genes

between C16:0-sensitive or 18:0-sensitive cells, a metabolism-associated gene ACSL5 or inflammation-associated gene CCL3 was identified in ADC or SCLC cells, respectively, on the basis of the top 10 highly expressed genes. ACSL5 encodes an enzyme acyl-CoA synthetase long-chain family member 5 related to fatty acid degradation and lipid biosynthesis (Ding et al. 2017) to activate fatty acids from exogenous sources and synthesize triacylglycerol for intracellular storage. The expression of ACSL5 gene varied among different tumors (Reinartz et al. 2010; Gassler et al. 2003; Hartmann et al. 2017). CSF2 plays key roles in immunomodulation and hematogenesis and acts as a tumor-derived factor to promote tumor growth and development (Hong 2016).

The interaction of target lipids with the corresponding genes is important to deeply understand potential mechanisms of sensitivity to metabolites, evidenced by the fact that C16:0 upregulated ACSL5 expression in ADC cells in a time- and dose-dependent pattern and the deletion of ACSL5 led to the occurrence of cell insensitivity. This indicates that ACSL5 plays a decisive role in the interaction between C16:0 and cells. ACSL5 is one of the five ACSL isoforms in mammals (e.g., ACSL1, ACSL3, ACSL4, ACSL5, and ACSL6) located in the mitochondria and contributes to cell apoptosis by alternative splicing (Gassler et al. 2007). ACSL5 expression was altered in bladder, esophagus, lung, pancreatic, and prostate cancer, due to the heterogeneity of its own genomic patterns and biological characteristics.

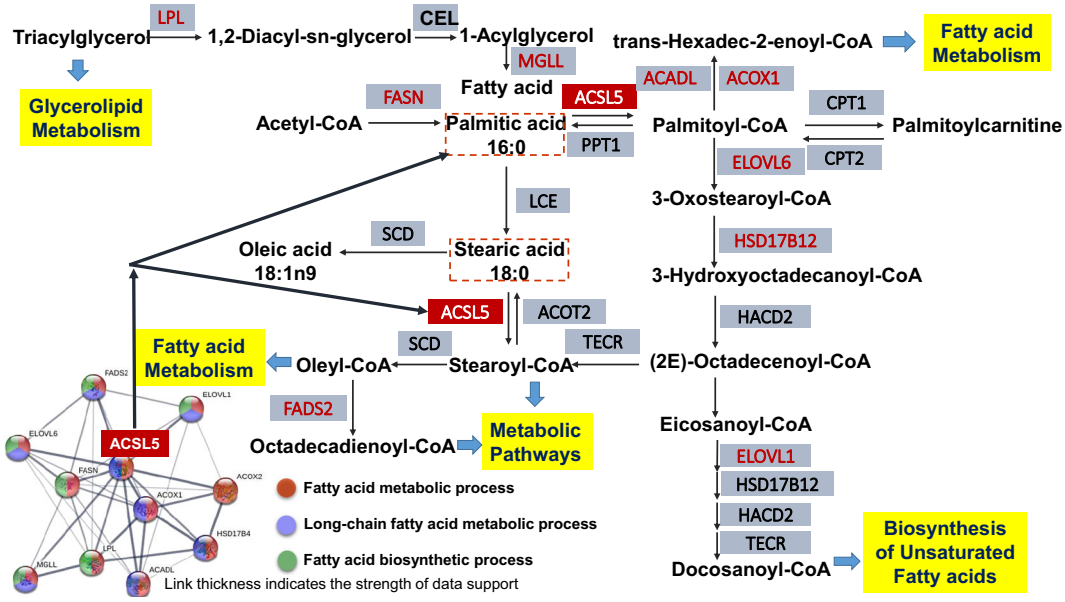

Fig. 8 Summary of molecular mechanisms by which palmitic acid and stearic acid interact with ACSL5 in the metabolic pathway and role of ACSL5-related proteins in metabolism. Triglycerides are catalyzed by LPL to 1,2-diacyl-sn-glycerol, metabolized to 1-acylglycerol by CEL, and catalyzed to fatty acid by MGLL. Palmitic acid is a type of fatty acid. Synthesis of palmitic acid by adding C atom by FASN multistep reaction of acetyl-CoA. Palmitic acid can be reacted to palmitoyl-CoA under the catalysis of ACSL5, and further CPT1 to palmitoylcarnitine. After CPT2 and PPT1, other enzymes can be catalyzed to palmitic acid again. Palmitic acid can also be converted to stearic acid via LCE. On the one hand, it can be catalyzed to oleic acid by SCD, or it can become stearoyl-CoA through ACSL5 and continue to be metabolized by SCD to oleyl-CoA and octadecadienoyl-CoA. On the other hand, palmitoyl-CoA can also be catalyzed to stearoyl-CoA by ELOVL6, HSD17B12, HACD2, and TECR, or it can continue to increase the C chain length to docosanoyl-CoA. In the protein–protein interaction network (PPI), almost all ACSL5-related enzymes play an important role in the metabolism of palmitic acid and stearic acid. Among them, FADS2, ELOVL6, ELOVL1, FASN, ACOX1, HSD17B4, and ACADL are related to fatty acid metabolism, ACOX2 is connected with bile acid metabolism, MGLL has connection with glyceride metabolism and LPL is related to cholesterol metabolism. LPL, lipoprotein lipase; CEL, carboxyl ester lipase; MGLL, monoglyceride lipase; FASN, fatty acid synthase; ACADL, acyl-CoA dehydrogenase long chain; ACOX1, acyl-CoA oxidase 1; PPT1, palmitoyl-protein thioesterase 1; CPT1, carnitine palmitoyltransferase 1; CPT2, carnitine palmitoyltransferase 2; ELOVL6, fatty acid elongase 6; LCE, long-chain elongase; SCD, sterol-CoA desaturase; HSD17B12, hydroxysteroid 17-beta dehydrogenase 12; ACTO2, acyl-CoA thioesterase 2; TECR, trans-2,3-enoyl-CoA reductase; HACD2, 3-hydroxyacyl-CoA dehydratase 2; FADS2, fatty acid desaturase 2; ELOVL1, fatty acid elongase 1

ACSL5 gene expression varies in different cancer types and even in different subclasses. The high expression of ACSL5 gene has a positive impact for prognosis of patients with breast, colorectal, lung, and ovarian cancer (Chen et al. 2016). ACSL5 is strongly involved in metabolism of palmitic acid, palmitoleic acid, oleic acid, and linoleic acid. The decrease of ACSL5 and Wnt family member 2B was related to the abnormality of lung development and the pathogenesis of human congenital pulmonary airway malformations (Qu et al. 2018). In addition, the present study demonstrated that C18:0 could upregulate CSF2 expression in SCLC cells in a time- and dose-dependent pattern to participate in cell sensitivity, which was altered by the deletion of the CSF2 gene.

Alterations of metabolism- or inflammation-associated CCL3 and PDK4 were functionally linked with CSF2 and ACSL5. C16:0 and C18:0 increased the expression of PDK4 gene in different patterns. For example, C16:0 gradually and consistently increased PDK4 expression paralleled with the expression of the ACSL5 gene, while C18:0-induced PDK4 overexpression appeared later than CSF2 changes. It indicates that PDK4 was associated with the inhibitory effects of target lipids in cell proliferation, probably being a primary, secondary, or additive factor during the interaction between target lipids and cells. ACSL5 plays an important role in the maintenance of intracellular energy and carnitine palmitoyl transferase 1A activity, which may be a critical mechanism by which C16:0 inhibited cell proliferation. However, CSF2 as one of the inflammatory factors also shows a decisive role in the process of C18:0-inhibited cell proliferation associated with the increase of intracellular energy. Different functions of ACSL5 and CSF2 have the same influence in the sensitivity of various lung cancer cells to different target lipids. For example, ACSL5 not only plays a central role in the associated gene networks in the processes of fatty acid and long-chain fatty acid metabolism and fatty acid biosynthesis, but also in the metabolic processes of palmitic acid and stearic acid through the control of the transfer from palmitic acids to palmitory-CoA and from stearic acids to stearoyl-CoA, as explained in Fig. 8. However, nonsensitive or co-sensitive cells are equally important for further studying the mechanism of lipid metabolism. In addition, the challenge of clinical trans-omics is to take more resources, research budgets, and processes to manage the comprehensive information and analyses, even though it becomes more important and adaptable to the clinic.

In conclusion, we identified lung cancer-specific, lung cancer subtype-specific, and clinical phenome-specific target lipid elements and integrated clinical phenomics, lipidomics, and transcriptomics to find lung cancer-specific and lung cancer subtype-specific target lipids palmitic acids (C16:0) or stearic acids (C18:0). The lung cancer subtype-specific trans-points/crossing-points between clinical phenomics and lipidomics network demonstrated an individual phenome corresponding to lipid(s) or lipid to phenome(s). C16:0 or C18:0 exhibited antiproliferative effects in sensitive cells with a time- and dose-dependent decline of cell proliferation. The metabolism-associated gene ACSL5 and inflammation-associated gene CCL3 were identified in ADC and SCLS to play decisive roles in cell sensitivity. C16:0 and C18:0 increased the expression of PDK4 gene in different patterns and inhibited cell proliferation through the alterations of intracellular energy. Thus, our data provide a new strategy to investigate the trans-points between clinical phenomics and lipidomics and target lipid-associated molecular mechanisms to benefit the discovery of new therapies.

Funding information The work was supported by operation funding of the Shanghai Institute of Clinical Bioinformatics and Shanghai Engineering and Technology Center for Artificial Intelligence of Lung and Heart Diseases from Zhongshan Hospital, The National Nature Science Foundation of China (81873409), and National Key Research and Development Program of Precision Medicine (2017YFC0909500).

Compliance with ethical standards

The study was approved by Zhongshan Hospital Ethics Committee of Fudan University.

References

Bligh EG, Dyer WJ. A rapid method of total lipid extraction and purification. Can J Biochem Physiol. 1959;37(8):911–7. https://doi.org/10.1139/o59-099.

Chen WC, Wang CY, Hung YH, Weng TY, Yen MC, Lai MD. Systematic analysis of gene expression alterations and clinical outcomes for long-chain acyl-coenzyme A synthetase family in cancer. PLoS One. 2016;11(5):e0155660. https://doi.org/10.1371/journal.pone.0155660.

Chen Y, Ma Z, Shen X, Li L, Zhong J, Min LS, et al. Serum lipidomics profiling to identify biomarkers for non-small cell lung cancer. Biomed Res Int. 2018;2018:5276240. https://doi.org/10.1155/2018/5276240.

Chirshev E, Oberg KC, Ioffe YJ, Unternaehrer JJ. Let-7 as biomarker, prognostic indicator, and therapy for precision medicine in cancer. Clin Transl Med. 2019;8(1):24. https://doi.org/10.1186/s40169-019-0240-y.

Ding S, Tang S, Wang M, Wu D, Guo H. Acyl-CoA synthetase 5 promotes the growth and invasion of colorectal cancer cells. Can J Gastroenterol Hepatol. 2017;2017:7615736. https://doi.org/10.1155/2017/7615736.

Doumandji Z, Safar R, Lovera-Leroux M, Nahle S, Cassidy H, Matallanas D, et al. Protein and lipid homeostasis altered in rat macrophages after exposure to metallic oxide nanoparticles. Cell Biol Toxicol. 2019:1–18. https://doi.org/10.1007/s10565-019-09484-6.

Gao D, Zhang L, Song D, Lv J, Wang L, Zhou S, et al. Values of integration between lipidomics and clinical phenomes in patients with acute lung infection, pulmonary embolism, or acute exacerbation of chronic pulmonary diseases: a preliminary study. J Transl Med. 2019;17(1):162. https://doi.org/10.1186/s12967-019-1898-z.

Gassler N, Schneider A, Kopitz J, Schnolzer M, Obermuller N, Kartenbeck J, et al. Impaired expression of acyl-CoA-synthetase 5 in epithelial tumors of the small intestine. Hum Pathol. 2003;34(10):1048–52. https://doi.org/10.1053/s0046-8177(03)00431-3.

Gassler N, Roth W, Funke B, Schneider A, Herzog F, Tischendorf JJ, et al. Regulation of enterocyte apoptosis by acyl-CoA synthetase 5 splicing. Gastroenterology. 2007;133(2):587–98. https://doi.org/10.1053/j.gastro.2007.06.005.

Han X, Gross RW. Shotgun lipidomics: multidimensional MS analysis of cellular lipidomes. Expert Rev Proteomics. 2005;2(2):253–64. https://doi.org/10.1586/14789450.2.2.253.

Han Y, Li L, Zhang Y, Yuan H, Ye L, Zhao J, et al. Phenomics of vascular disease: the systematic approach to the combination therapy. Curr Vasc Pharmacol. 2015;13(4):433–40.

Hartmann F, Sparla D, Tute E, Tamm M, Schneider U, Jeon MK, et al. Low acyl-CoA synthetase 5 expression in colorectal carcinomas is prognostic for early tumour recurrence. Pathol Res Pract. 2017;213(3):261–6. https://doi.org/10.1016/j.prp.2016.09.002.

Hong IS. Stimulatory versus suppressive effects of GM-CSF on tumor progression in multiple cancer types. Exp Mol Med. 2016;48(7):e242. https://doi.org/10.1038/emm.2016.64.

Lin L, Ding Y, Wang Y, Wang Z, Yin X, Yan G, et al. Functional lipidomics: palmitic acid impairs hepatocellular carcinoma development by modulating membrane fluidity and glucose metabolism. Hepatology. 2017;66(2):432–48. https://doi.org/10.1002/hep.29033.

Lv J, Gao D, Zhang Y, Wu D, Shen L, Wang X. Heterogeneity of lipidomic profiles among lung cancer subtypes of patients. J Cell Mol Med. 2018a;22(10):5155–9. https://doi.org/10.1111/jcmm.13782.

Lv J, Zhang L, Yan F, Wang X. Clinical lipidomics: a new way to diagnose human diseases. Clin Transl Med. 2018b;7(1):12. https://doi.org/10.1186/s40169-018-0190-9.

Mirtavoos-Mahyari H, Ghafouri-Fard S, Khosravi A, Motevaseli E, Esfahani-Monfared Z, Seifi S, et al. Circulating free DNA concentration as a marker of disease recurrence and metastatic potential in lung cancer. Clin Transl Med. 2019;8(1):14. https://doi.org/10.1186/s40169-019-0229-6.

Qi X, Yu C, Wang Y, Lin Y, Shen B. Network vulnerability-based and knowledge-guided identification of microRNA biomarkers indicating platinum resistance in high-grade serous ovarian cancer. Clin Transl Med. 2019;8(1):28. https://doi.org/10.1186/s40169-019-0245-6.

Qiao T, Wang X. A new light of proteomics in cell biology and toxicology. Cell Biol Toxicol. 2019;35(4):289–91. https://doi.org/10.1007/s10565-019-09492-6.

Qu Y, Liu D, Jia H, Zhou X. Expression analysis of ACSL5 and Wnt2B in human congenital pulmonary airway malformations. J Surg Res. 2018;232:128–36. https://doi.org/10.1016/j.jss.2018.06.023.

Reinartz A, Ehling J, Leue A, Liedtke C, Schneider U, Kopitz J, et al. Lipid-induced up-regulation of human acyl-CoA synthetase 5 promotes hepatocellular apoptosis. Biochim Biophys Acta. 2010;1801(9):1025–35. https://doi.org/10.1016/j.bbalip.2010.04.010.

Wang X. Clinical trans-omics: an integration of clinical phenomes with molecular multiomics. Cell Biol Toxicol. 2018;34(3):163–6. https://doi.org/10.1007/s10565-018-9431-3.

Wang X, Zhang Y, Nilsson CL, Berven FS, Andren PE, Carlsohn E, et al. Association of chromosome 19 to lung cancer genotypes and phenotypes. Cancer Metastasis Rev. 2015;34(2):217–26. https://doi.org/10.1007/s10555-015-9556-2.

Xu M, Wang DC, Wang X, Zhang Y. Correlation between mucin biology and tumor heterogeneity in lung cancer. Semin Cell Dev Biol. 2017;64:73–8. https://doi.org/10.1016/j.semcdb.2016.08.027.

Yan F, Zhao H, Zeng Y. Lipidomics: a promising cancer biomarker. Clin Transl Med. 2018;7(1):21. https://doi.org/10.1186/s40169-018-0199-0.

Yugi K, Kubota H, Hatano A, Kuroda S. Trans-omics: how to reconstruct biochemical networks across multiple 'omic' layers. Trends Biotechnol. 2016;34(4):276–90. https://doi.org/10.1016/j.tibtech.2015.12.013.

Zemski Berry KA, Murphy RC, Kosmider B, Mason RJ. Lipidomic characterization and localization of phospholipids in the human lung. J Lipid Res. 2017;58(5):926–33. https://doi.org/10.1194/jlr.M074955.

Zerin T, Kim JS, Gil HW, Song HY, Hong SY. Effects of formaldehyde on mitochondrial dysfunction and apoptosis in SK-N-SH neuroblastoma cells. Cell Biol Toxicol. 2015;31(6):261–72. https://doi.org/10.1007/s10565-015-9309-6.

Zhang L, Han X, Wang X. Is the clinical lipidomics a potential goldmine? Cell Biol Toxicol. 2018;34(6):421–3. https://doi.org/10.1007/s10565-018-9441-1.

Zhang L, Zhu B, Zeng Y, Shen H, Zhang J, Wang X. Clinical lipidomics in understanding of lung cancer: opportunity and challenge. Cancer Lett. 2020;470:75–83. https://doi.org/10.1016/j.canlet.2019.08.014.